Plasma Transport Theory Spanning Weak to Strong Coupling

Jérôme Daligault[*] and Scott D. Baalrud[†]

[*]*Theoretical Division, Los Alamos National Laboratory, Los Alamos, New Mexico 87545, USA*
[†]*Department of Physics and Astronomy, University of Iowa, Iowa City, Iowa 52242, USA*

Abstract. We describe some of the most striking characteristics of particle transport in strongly coupled plasmas across a wide range of Coulomb coupling strength. We then discuss the effective potential theory, which is an approximation that was recently developed to extend conventional weakly coupled plasma transport theory into the strongly coupled regime in a manner that is practical to evaluate efficiently.

INTRODUCTION

The goal of this paper is twofold. Firstly, to give an overview of salient features of transport mechanisms across regimes of coupling; from the weakly coupled gas-like regime, to the very strongly coupled liquid-like regime. Secondly, to present the "effective potential theory", a physically intuitive theory based on a Boltzmann-like binary collision picture that was recently developed by the authors for extending traditional plasma transport theories into the strong coupling regime.

We focus on the transport properties of classical ions in strongly coupled plasmas. For simplicity, we use the one-component plasma (OCP) model to illustrate the subject. The OCP, which is the reference model in the study of strongly-coupled Coulomb systems, consists of a three dimensional infinite system of particles of electric charge q, mass m and particle density n, interacting through the bare Coulomb interactions, and immersed in a uniform neutralizing background [1]. The OCP is remarkable in that its equilibrium and near-equilibrium properties depend on a single parameter, the Coulomb coupling parameter $\Gamma = \frac{q^2/a}{k_B T}$. This is defined as the ratio of the mean potential energy per particle q^2/a, where $a = (3/4\pi n)^{1/3}$ is the Wigner-Seitz radius, divided by the mean kinetic energy per particle $k_B T$, where T is the temperature and k_B is the Boltzmann constant. The Coulomb coupling parameter measures the degree of non-ideality of the system, i.e. the degree to which many-body interactions affect the properties of the ensemble of ions. As Γ increases, the OCP dynamics shows transitions from a nearly collisionless, gaseous regime for $\Gamma \ll 1$ continuously through an increasingly correlated, liquid-like regime at Γ above 50. At $\Gamma = 175$, the OCP undergoes a first-order fluid-solid phase transition. By varying Γ, the OCP exhibits the various facets of strong coupling effects on the transport properties, which we will highlight in the next section. Movies of molecular dynamics simulations illustrating these different regimes may be viewed at the authors' webpage [2].

SALIENT FEATURES OF THE OCP TRANSPORT PROPERTIES ACROSS COUPLING REGIMES

In the following paragraphs, we describe what characterizes the transport properties in the various regimes of the fluid phase. While the OCP has one fluid phase only (there is no gas-liquid phase transition), it is nevertheless possible to identify at least three distinctive regimes in the transport properties: firstly, a dilute gas-like, weakly coupled regime for $\Gamma < 0.1$; secondly, a liquid-like, strongly coupled regime for $\Gamma \geq 50$; and finally, a gas-like to liquid-like crossover regime for intermediate coupling strengths.

Weakly coupled regime

The weakly coupled regime is the realm of traditional plasma physics. Here particle dynamics is controlled by their considerable kinetic energy, which gives rise to a large mobility. This is often compared to the mobility of neutral particles in a dilute gas. In the case of neutral gases, the interaction potential is short-range and particle dynamics is well described as a succession of occasional, uncorrelated, large-angle binary collisions; a process well described by the Boltzmann kinetic equation. For charged particles in a weakly coupled plasma, however, the potential is long-range. Particles mostly undergo a succession of infinitesimal deflections because interactions occur via the tail of a Coulomb potential that is screened by the polarization of background particles. Strong (large angle) deflections are much less frequent in weakly coupled plasmas. This dynamics is more appropriately described with the Landau equation, which can be regarded as an approximation of the Boltzmann equation obtained by keeping only the small angle, grazing collisions. In the process, an integral $\int \frac{db}{b}$ over all possible impact parameters b appears that is divergent at both ends of the integration range: at small impact parameter because of the grazing collisions approximation, and at large impact parameter because the calculation is done assuming a bare Coulomb interaction, which does not account for particle screening. In practice, physically-motivated cutoff parameters are introduced to regularize the otherwise divergent integral, which defines the so-called Coulomb logarithm $\ln \Lambda = \int_{b_{min}}^{b_{max}} \frac{db}{b} = \ln(b_{max}/b_{min})$: the smallest impact parameter is set to the distance of closest approach $b_{min} = q^2/k_B T$, and the largest impact parameter is equaled to the Debye-Hückel screening length $b_{max} = \sqrt{k_B T/4\pi n q^2}$. In terms of the dimensionless parameter Γ,

$$\ln \Lambda = \ln \frac{1}{\sqrt{3}\Gamma^{3/2}} . \tag{1}$$

By solving the Boltzmann or Landau equations with, for instance, the Chapman-Enskog method, one obtains explicit expressions for the transport coefficients that enter the hydrodynamic equations that describe the system's dynamics on macroscopic scales. These coefficients essentially depend on the interaction potential $v(r)$ through the scattering angle,

$$\Theta = b \int_{r_0}^{\infty} \frac{dr}{r^2} \frac{1}{\sqrt{1 - \frac{b^2}{r^2} - \frac{4m}{|\mathbf{p}-\mathbf{p}'|^2} v(r)}} , \tag{2}$$

in which $|\mathbf{p} - \mathbf{p}'|$ is the magnitude of the relative particle momenta, and r_o is obtained from the largest root of the denominator. At lowest order in the Chapman-Enskog solution, one obtains the traditional Landau-Spitzer formulas for the self-diffusion coefficient D,

$$D^* = \frac{D}{a^2 \omega_p} = \sqrt{\frac{\pi}{3}} \frac{1}{\Gamma^{5/2} \ln \Lambda} \tag{3}$$

or the shear-viscosity coefficient η,

$$\eta^* = \frac{\eta}{mna^2 \omega_p} = \frac{5}{3} \sqrt{\frac{\pi}{3}} \frac{1}{\Gamma^{5/2} \ln \Lambda} \tag{4}$$

in terms of the Coulomb logarithm. These are found in most plasma physics textbooks.

Recently, the progress in computer hardware has allowed the direct validation of the admitted Landau-Spitzer results. Figure 1 shows the shear-viscosity coefficient η^* as a function of the coupling parameter Γ obtained with highly accurate molecular dynamics (MD) simulations [3] (red crosses) and with the Landau-Spitzer formula (4) (orange full line). In the MD simulations, N particles are placed in a cubic box of volume $V = L^3$ and periodic conditions are imposed on all boundaries. Particle trajectories are determined by solving Newton's equations of motion with the velocity Verlet integrator Our timestep $\delta t = 10^{-2}/\omega_p$ is chosen small enough to ensure excellent energy conservation for all Γ values. In all simulations, $N = 5000$ for $\Gamma > 0.5$, while $N = 50000$ was chosen for $\Gamma < 0.5$ to ensure high enough collisionality in the simulation cell.

In the weakly coupled regime $\Gamma < 0.1$, the Landau-Spitzer result (4) lies slightly higher than the MD data. The Landau-Spitzer result (4) can be corrected to match the MD data by multiplying the expression by a coefficient of order one and by multiplying the factor Λ in the logarithm by another parameter of order one. The first factor is a correction to the fact that the formula (4) corresponds to the lowest-order Chapman-Enskog expansion of the
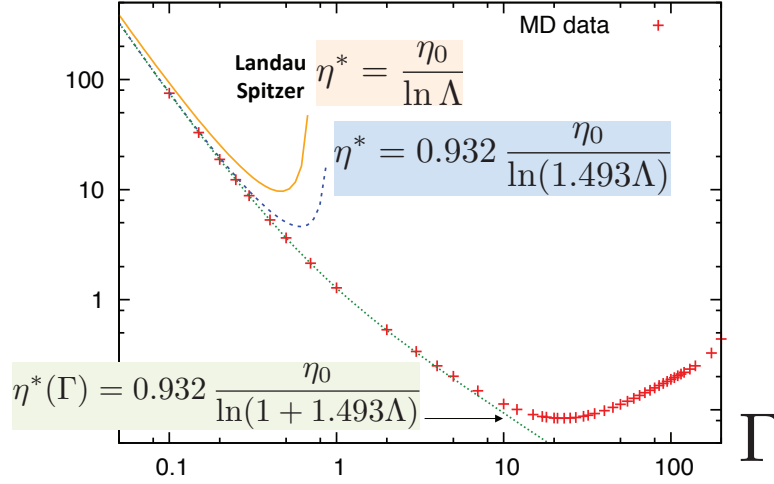
FIGURE 1. (color online) Dimensionless shear-viscosity coefficient $\eta^* = \frac{\eta}{mna^2\omega_p}$ of the OCP obtained with molecular dynamics simulations (red crosses), the Landau-Spitzer formula (4) (orange line) with $\eta_0 = \frac{5}{3}\sqrt{\frac{\pi}{3}}\frac{1}{\Gamma^{5/2}}$, and the corrected Landau Spitzer formulas (green dotted line) that extends the original Landau-Spitzer formula in the moderately coupled regime.
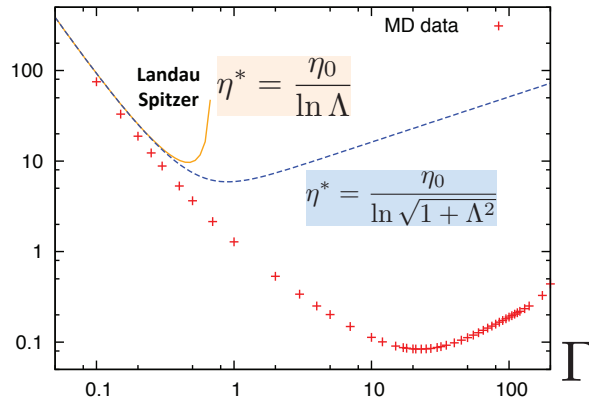

FIGURE 2. (color online) Dimensionless shear-viscosity coefficient $\eta^* = \frac{\eta}{mna^2\omega_p}$ of the OCP obtained with molecular dynamics simulations (red crosses), the Landau-Spitzer formula (4) (orange line) with $\eta_0 = \frac{5}{3}\sqrt{\frac{\pi}{3}}\frac{1}{\Gamma^{5/2}}$, and the ansatz (6).

Landau kinetic equation. This can be computed from higher order terms in the expansion. The second correction is associated with inaccuracy of the ad-hoc cutoff parameters (b_{min} and b_{max}) that are used in Landau's determination of the Coulomb logarithm. These corrections are well understood and have been derived from various approaches, including the effective potential theory described below [4]. With these corrections, the Landau-Spitzer formula is in very good agreement with the MD data up to Γ values around $0.1 - 0.2$, beyond which it diverges. In other words, beyond $\Gamma \approx 0.1$, conventional plasma theory, which neglects the effects of strong Coulomb coupling, breaks down.

The Landau-Spitzer result can be extended in an *ad-hoc* manner to higher Γ values. The green dashed line in Fig. 1 shows that by adding 1 in the argument of the Coulomb logarithm the resulting modified Landau-Spitzer model extends to the moderately coupled regime to high accuracy up to $\Gamma < 8 - 10$. In fact, we have found that this simple correction works equally well for all the transport properties that we have studied, including the self- and mutual-diffusion coefficients of mixtures and the temperature relaxation rate in electron-ion plasmas [5]. In other words, the Landau-Spitzer expression $T = T_0/\ln\Lambda$ for a transport property T can be empirically extended to the moderately
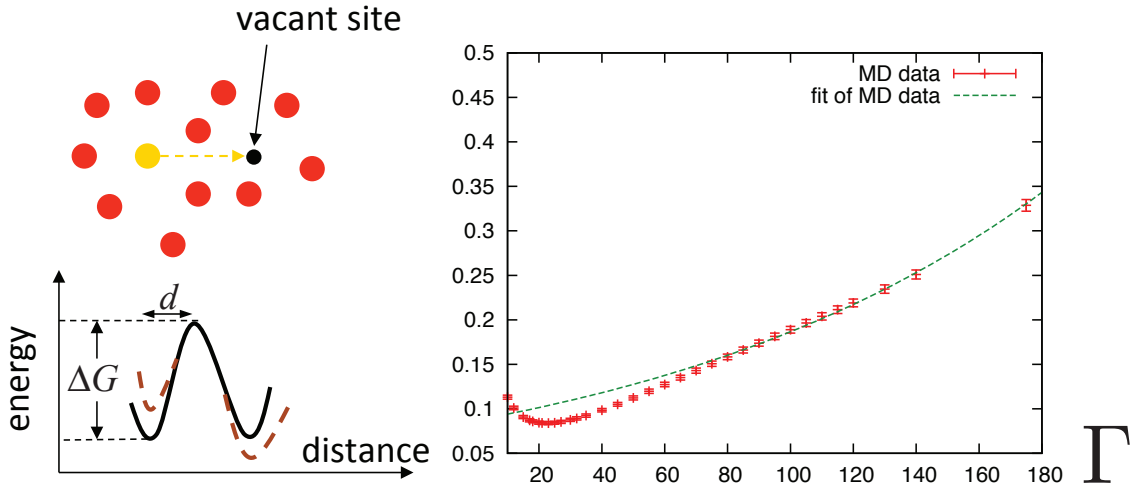
FIGURE 3. (color online) Left panel: Cartoon illustration of the cage model. Right panel: Dimensionless shear-viscosity coefficient $\eta^* = \frac{\eta}{mna^2\omega_p}$ of the OCP obtained with MD simulations (red crosses). The green line show a least-square fit at large Γ of the MD data with a fitting formula of the form (8) predicted by Eyring; in dimensionless units, the fitting formula is $\eta^*(\Gamma) = ae^{b\Gamma}$, and a least-square fit over the range $\Gamma \geq 60$ gives $a \approx 0.087$ and $b \approx 0.00762$. The MD data are represented with error bars of 5%.

coupled regime as follows, where the factors α and β are of order 1,

$$T = \frac{\alpha T_0}{\ln(1 + \beta\Lambda)}. \tag{5}$$

In the literature, some authors advocate this expression [6]

$$T = \frac{T_0}{\ln\sqrt{(1 + \Lambda^2)}} \tag{6}$$

to extend the domain of validity of Landau-Spitzer. The latter remains non-negative and non-divergent for all Γ but, as shown in Fig. 2, its accuracy beyond the range $\Gamma < 0.1$ is poor.

Strongly coupled regime

At coupling strengths above 50, strong interparticle interactions give rise to the cage-effect [7, 8], whereby, as illustrated in Fig. 3, each particle finds itself trapped for some period of time in the cage formed by its immediate neighbors, rebounding until it overcomes the energy barrier and diffuses to a neighboring cage. The cage effect is typical of neutral liquids. And indeed, despite the strong collective longitudinal oscillations that affect the microscopic dynamics, the OCP displays many characteristics of neutral liquids when looking at transport properties that occur on a long, hydrodynamic time-scale. For instance, the self-diffusion and the shear-viscosity coefficients satisfy the Stokes-Einstein relation, according to which the product of the self-diffusion and the viscosity divided by the temperature is constant. For the OCP, MD data for self-diffusion and shear-viscosity coefficients give

$$\frac{4\pi a}{k_B T} D\eta \approx 0.34 \quad , \quad \Gamma > 50. \tag{7}$$

Another example of liquid-like behavior is the scaling of the viscosity with temperature. At high Gamma, the viscosity satisfies an Arrhenius-like relation,

$$\eta = \tilde{\eta} e^{\frac{\Delta G}{k_B T}} , \tag{8}$$

i.e., it is proportional to the exponential of an energy ΔG divided by $k_B T$. This behavior can be understood with the old model that Eyring developed in the 1930 's, which relies on the cage effect [9]. The approach is based on the absolute reaction rates theory that is widely used in chemistry, in which a cage is represented by an energy barrier ΔG, as illustrated in Fig. 3. The frequency at which a caged particle can overcome and pass the potential barrier is given by

$$\nu = \kappa k_B T e^{-\frac{\Delta G}{k_B T}} \tag{9}$$

where κ is an unknown factor that describes the geometry of a cage. From this, Eyring inferred an expression like (8) for the shear-viscosity coefficient. The OCP viscosity does behave as predicted by Eyring at very large Γ, and from the fit of the data with Eq.(8) we can infer information on the cage effect: for instance, we find that the height of the cage scales like $\Delta G = 1.33 T_m$, where T_m is the melting temperature.

Intermediate regime

Less is known about the transition region between the weakly-coupled gas-like regime and the strongly-coupled liquid-like regime. In this region, both kinetic and interaction effects influence momentum and energy transport. In Fig. 1, one sees that the viscosity decreases with Γ, reaches a minimum around $\Gamma = 20$ and then increases again. The minimum results from the competition between kinetic and interaction effects. Indeed, in a fluid, transport of momentum occurs not only by bodily motion, but also by direct transmission of intermolecular forces. This can be seen in the expression for the microscopic stress tensor,

$$\sigma(t) = \sum_{i=1}^{N} m\mathbf{v}_i(t)\mathbf{v}_i(t) + \sum_{i=1}^{N} \mathbf{F}_i(t)\mathbf{r}_i(t) \tag{10}$$
$$= \text{kinetic term} + \text{potential term} \tag{11}$$

which consists of the sum of a kinetic part and an interaction part ($\mathbf{r}_i(t)$ is the position of particle i at time t, $\mathbf{v}_i(t)$ its velocity and $\mathbf{F}_i(t)$ the force acting on it due to its interactions with all other particles.)

Movies of molecular dynamics simulations (accessible at the url address given in the introduction) clearly show that particles cruise through the entire system less and less easily as they undergo an increasingly larger number of deflections that hamper their mobility. But nevertheless, overall, the individual particle dynamics still looks as a succession of binary collisions. This remark is the basis for the effective potential theory that we have recently developed in order to extend the traditional theory of Landau-Spitzer to the strongly coupled regime.

THE EFFECTIVE POTENTIAL THEORY

The basis of the effective potential theory is still the binary collision picture of Boltzmann, but now instead of using the bare Coulomb interaction $v(r)$, we describe the interaction between two particles via an effective potential $\phi(r)$ that incorporates key features of the many-body-correlations that can no-longer be neglected at high coupling. This approach can be regarded as a renormalization of the interaction potential of two particles due to the presence of other surrounding particles according to the scheme

"bare" interaction $v(r)$ + interactions with environment $\rightarrow$ "effective, dressed" interaction $\phi(r)$.

The effective potential $\phi(r)$ is then directly used in the Boltzmann equation and in particular in the Chapman-Enskog expressions of the transport coefficients: for instance, in the scattering angle formula (2), the Coulomb potential is substituted for the effective potential as follows,

$$\Theta = b \int_{r_0}^{\infty} \frac{dr}{r^2} \frac{1}{\sqrt{1 - \frac{b^2}{r^2} - \frac{4m}{|\mathbf{p}-\mathbf{p}'|^2}\phi(r)}} , \tag{12}$$

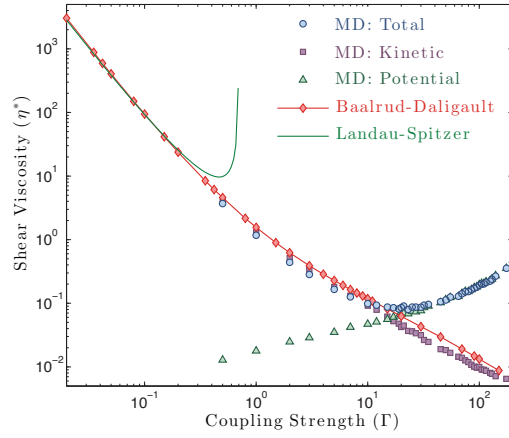and the transport coefficients are evaluated with this modified scattering angle.

FIGURE 4. (color online) Contributions to the shear-viscosity coefficient computed from MD: kinetic η_{kk} (purple squares), potential η_{pp} (green triangles), and total (blue circles) η, all in reduced units. Also shown is the corrected Landau-Spitzer formula $\eta = 0.932\eta_0/\ln(1.493\Lambda)$ (green line) and the effective potential theory (red diamonds).

The effective potential is defined as follows. Consider at some instant of time, the force on a given particle, say particle 1: it is the gradient of the interaction energy $U(\mathbf{r}_1, \mathbf{r}_2, \ldots, \mathbf{r}_N,)$ with all the other particles 2, 3, 4 and so on and so forth. If one weighs this microscopic force with the probability to find the particles in spatial configuration $(\mathbf{r}_1, \ldots, \mathbf{r}_N)$, which at thermal equilibrium is given by the normalized Boltzmann factor $e^{-U/k_BT}/Q$ with Q the configuration partition function, and then integrates over positions r_3, r_4 and so on, one obtains the average force $\langle \mathbf{F}_{12} \rangle$ between particles 1 and 2 in the presence of all other particles, i.e.

$$\langle \mathbf{F}_{12} \rangle = \int -\nabla_{\mathbf{r}_1} U \frac{e^{-U/k_BT}}{Q} d\mathbf{r}_3 \ldots d\mathbf{r}_N . \tag{13}$$

What is remarkable is that it is possible to rewrite this average in terms of the pair-distribution function g(r) as $\langle \mathbf{F}_{12} \rangle = -k_BT\nabla_{\mathbf{r}_1} \ln g(|\mathbf{r}_1 - \mathbf{r}_2|)$, i.e. the average force between 1 and 2 is equal to k_BT times the gradient of the logarithm of the pair distribution function (physically, $ng(r)$ represents the radial density profile around an individual particle). So the average force between 1 and 2 is equal to the gradient of a potential ϕ, which is related to the pair-distribution function through the Boltzmann-type relation,

$$g(r) = e^{-\phi(r)/k_BT} . \tag{14}$$

The potential $\phi(r)$ is known as the potential of mean force.

We chose ϕ to be the effective potential of the effective potential theory. Hence $g(r)$ is the only input of the theory. To calculate ϕ, we need to know $g(r)$. Fortunately there exists very accurate simple models for calculating $g(r)$, such as the hypernetted-chain (HNC) approximation [10]. Note that the theory can be extended to deal with mixtures [11], in which case the only inputs are the mutual pair distribution function between the different pairs of particle species: $\phi_{ij}(r) = -k_BT \ln g_{ij}(r)$.

We now discuss how our physically motivated theory compares with accurate simulation data, starting with the shear-viscosity coefficient. On Fig. 4, we show the MD results for the reduced shear viscosity coefficient as a function of the coupling strength Γ already presented in Fig. 1. The latter was obtained by evaluating the Kubo formula

$$\eta = \frac{1}{6Vk_BT} \sum_{x<y} \int_0^\infty dt \langle \sigma_{xy}(t)\sigma_{xy}(0) \rangle \tag{15}$$

that gives the viscosity coefficient in terms of the time integral of the stress tensor autocorrelation function. Using (10), $\eta \approx \eta_{kk} + \eta_{pp}$, where the contribution of the autocorrelation of the kinetic part of the stress tensor is shown in purple in Fig. 4, while the contribution of the autocorrelation of the interaction part is shown in green (there is a kinetic-potential cross term that is not shown here because it is negligible). Figure 4 shows that at small Γ the shear viscosity is dominated by the kinetic part, and that at large Γ it is dominated by the interaction part. The competition
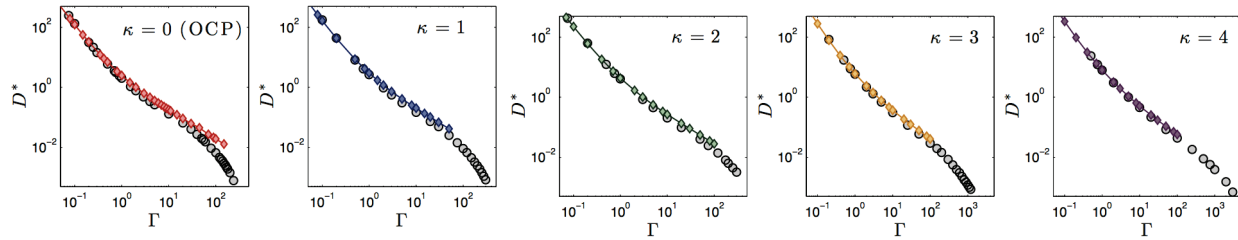
FIGURE 5. (color online) Self-diffusion coefficients of Yukawa OCP's at several values of the dimensionless inverse screening length $\kappa = a/\lambda_{sc}$ (in a Yukawa OCP, particles interact through the exponentially screened Coulomb potential $v(r) = q^2 \exp(-r/\lambda_{sc})/r$, where the parameter λ_{sc} mimics the effect of electronic screening). In each frame, the circles show molecular dynamics results and the diamonds show the prediction of the effective potential theory.
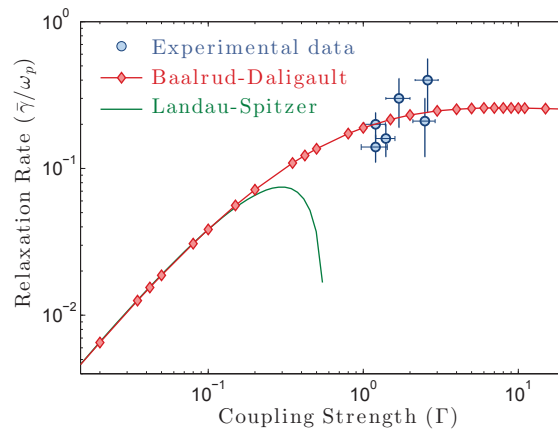

FIGURE 6. (color online) Comparison of the velocity relaxation rate measured in [14] (blue circles) with the theoretical predictions of the effective potential theory (red diamonds).

between kinetic and interaction effects leads to a minimum of shear-viscosity at intermediate Γ values around $\Gamma \approx 20$. We now compare the MD results with the prediction of the effective potential theory. The red line in Fig. 4 shows the result of the effective potential theory, the green line shows the corrected Landau-Spitzer result discussed earlier. The effective potential theory does very well at small gamma and, unlike the Landau-Spitzer result, remains in good agreement with the MD data up to Γ around 20-30. It then breaks down, because the Boltzmann equation on which it is based does not have any potential part, the momentum transport is kinetic. Note that the effective potential theory remains in agreement with the kinetic part at large gamma values.

We also find good agreement for the self-diffusion coefficient. In Fig. 5, we compare the effective potential theory with molecular dynamics simulation results for various Yukawa OCP where the bare Coulomb interaction is replaced by an exponentially screened Coulomb interaction to mimic electronic screening: our theory has the correct weakly coupled limit and agrees well with the simulation data up to $\Gamma = 50$. We also found good agreement for the temperature relaxation rate between electron and ions in electron-ion plasmas (not shown) [12, 13].

Finally, our theory is in good agreement with the measurements by the group of Prof. Killian at Rice University of the velocity relaxation in strongly-coupled ultracold plasmas. As can be seen in Fig. 6, while the Landau-Spitzer prediction for the relaxation rate breaks down around coupling of 0.1, our theory is within the error bars of the experimental measurements.

The effective potential theory does well but is not perfect. In all the calculations we have made, we find a systematic, approximately 30% underestimation of the collision rate in the range $1 \leq \Gamma \leq 50$. In the talk, we showed that a large part of the discrepancy can be removed if one accounts for the short-range correlations in the particle positions that are neglected in the molecular chaos assumption underlying the Boltzmann equation on which the effective potential theory is based. We have recently markedly improved the effective potential theory to include such effects using ideas developed by Enskog to deal with hard-spheres systems. The work was just submitted for publication and will not be

discussed here any further here.

ACKNOWLEDGMENTS

REFERENCES

1. M. Baus, and J.-P. Hansen, *Phys. Reports* **59**, 1 (1980).
2. Dense plasma theory webpage, `http://www.lanl.gov/projects/dense-plasma-theory/research/one-component-plasma.php` (2015).
3. J. Daligault, K. Rasmussen, and S. Baalrud, *Phys. Rev. E* **90**, 033105 (2014).
4. S. D. Baalrud, *Phys. Plasmas* **19**, 030701 (2012).
5. J. Daligault, *Phys. Rev. Lett.* **108**, 225004 (2012).
6. M. W. C. Dharma-wardana, and F. Perrot, *Phys. Rev. E* **58**, 3705 (1998).
7. Z. Donko, G. J. Kalman, and K. I. Golden, *Phys. Rev. Lett.* **88**, 225001 (2002).
8. J. Daligault, *Phys. Rev. Lett.* **96**, 065003 (2006).
9. H. Eyring, *J. Chem. Phys.* **4**, 283 (1936).
10. J.-P. Hansen, and I. R. McDonald, *Theory of Simple Liquids, 3rd Edition*, Academic Press, Oxford, 2006.
11. M. V. Beznogov, and D. G. Yakovlev, *Phys. Rev. E* **90**, 033102 (2014).
12. S. D. Baalrud, and J. Daligault, *Phys. Rev. Lett.* **110**, 235001 (2013).
13. S. D. Baalrud, and J. Daligault, *Phys. Plasmas* **21**, 055707 (2014).
14. G. Bannasch, J. Castro, P. McQuillen, T. Pohl, and T. C. Killian, *Phys. Rev. Lett.* **109**, 185008 (2012).